Combust. Sci. and Tech., 179: 2255–2278, 2007

ISSN: 0010-2202 print/1563-521X online
DOI: 10.1080/00102200701407911

Taylor & Francis
Taylor & Francis Group

Control of Heat Release and NO Emissions in a Combustor Through Modulation of Transverse Air-Jets

Onur Tuncer, Sumanta Acharya*, Jong Ho Uhm
Department of Mechanical Engineering Louisiana State University,
Baton Rouge, LA, USA

Abstract: The effect of modulated air jets, introduced through the combustor shell, on the temperature distribution and nitric oxide emissions is investigated. Temperature and emissions measurements have been made at a number of forcing frequencies in the range of 100–850 Hz, blowing ratios in the range of 4–10 and equivalence ratios between 0.6 and 1.0. Open-loop flame response to forcing has also been acquired by recording pressure spectra. Results show that substantial reductions in nitric oxide emissions index (15–30%) can be obtained over a wide range of flow conditions with side-air jet forcing. In addition, forcing also alters the time averaged temperature field, with higher mean temperatures close to the dump plane, due to enhanced fuel-air mixing. The higher temperatures and volumetric heat release obtained with forcing can enable more compact combustor designs. The lower emissions are potentially linked to greater unsteadiness with forcing.

Keywords: Emissions; Forced jet; Mixing; Spray combustion

Received 28 February 2006; accepted 12 April 2007.

This experimental study was supported by a grant from the ONR Propulsion program with Dr. Gabriel Roy as the program monitor, and by the Louisiana Board of Regents through the Clean Power and Energy Research Consortium (CPERC). This support is gratefully acknowledged. The help and support received from Mr. Jeffrey Willbanks in the various facets of the work is also acknowledged. Authors also would like to thank the editor and anonymous reviewers for their comments that helped to improve this article.

*Address correspondence to acharya@me.lsu.edu

INTRODUCTION

Volumetric heat release, pattern factors and emissions are three key performance metrics for contemporary propulsion systems and gas turbine combustors (Tuner et al., 2003, 2005). These metrics are usually a function of stoichiometry, degree of air fuel mixedness and also a function of the level of unsteadiness in the reacting flow. In a typical non-premixed can combustor geometry liquid fuel droplets are injected at the center of the dump plane and a swirling air provides mixing of reactants and hence better flame stabilization. In some combustor designs, additional side air jets are introduced radially through the combustor wall. These side air jets are used to control the local stoichiometry, and the fuel-air mixedness in the combustor. Proper utilization of these side air-jets can potentially lead to improvements in the performance metrics.

Turbulent jets in a cross-flow have been shown to favorably affect entrainment and mixing processes (Bicen, et al., 1990; Blossey et al., 2001; Crocker et al., 1994; Cho et al., 1998; Cortolezzi and Karagozian 2001; Griebel et al., 1997; Holdeman et al., 1996; Holdeman, 1993; Johari et al., 1999; Karagozian et al., 2002; Lilley 2002; McManus and Lo, 1995; Narayanan et al., 2002; Tuncer et al., 2003, 2005; Vermuelen and Yu, 1985; Vermuelen et al., 1986) in the cross-flow. Acoustic forcing of a confined jet triggers certain modes of vortex instabilities and alters/enhances the vortical structures of the jet leading to enhanced mixing (Vermulan et al., 1982; Vermuelen and Yu, 1985; Vermuelen et al., 1986; Cho et al., 1998; Johari et al., 1999; Blossey et al. 2001; Karagozian et al., 2002; Narayanan et al., 2002; Tuncer, 2003). Since small-scale mixing between fuel and air controls the heat release and the temperature distribution, modulation of the control air-jet can be considered as a possible strategy for combustion control, and holds promise for improvement of key performance merits. Passive design techniques [Crocker et al., 1994] can neither adapt to changes in load conditions, nor can they adapt to slow changes in system parameters due to aging. For example there are two categories of approaches for controlling the emission of nitric oxide from combustion sources; combustion and post-combustion techniques (Kim et al., 2001). As NO emission is heavily influenced by combustion parameters a desirable way of controlling its emission is to alter the combustion process. This work explores the feasibility of actively modulating the side air jets in order to control the fuel-air mixing so as to increase the volumetric heat release and to decrease emissions.

Numerous cold flow studies that explore the effects of side-air jet injection in a combustor have been reported in the literature. A parametric study has been performed by Holdeman et al. (1993, 1996) where an empirical self-similarity parameter (also known as Holdeman parameter) has been defined. An experimental investigation of isothermal round jet

discharging into a swirling cross flow has been reported by Lilley (2002). The effect of active control in a combustor was studied by Vermeulen et al. (1982, 1985, 1986), who demonstrated that the fuel-air mixing and exit plane temperature distribution can be modified by acoustic modulation of the dilution jets. Although improvement in mixing was observed, the outcome was moderate, with a temperature difference in the order of 10°C (Vermeulen et al., 1982). Tuncer et al. (2003, 2005) were able to demonstrate substantially greater variations in temperature (order of 100–200°C) with modulation of the primary air-jet in a model combustor. However, no emission measurements were reported in their study.

The goal of the present experimental study is to manipulate fuel-air mixing and unsteadiness in a swirl-stabilized spray combustor through modulation of side or transverse-air jets, and to examine the impact of this manipulation on pattern factor, volumetric heat release and nitric oxide emissions. Enhancements in these performance merits are important for a variety of reasons: (i) Lower pattern factor implies more uniform temperature distributions and elimination of hot spots (ii) Lower nitric oxide emissions are necessary for meeting increasingly stringent emission standards, and (iii) enhanced fuel-air mixing leading to higher volumetric heat release enables the design of more compact combustors. In this article, the nitric oxide emissions issue is the primary focus. This was not considered in the previous study (Tuncer et al., 2003, 2005) reported by the authors.

EXPERIMENTAL APPARATUS

A schematic of the experimental setup depicting all major components is provided in Figure 1. The combustor is cylindrical in shape with a diameter of $D = 194$ mm and a non-dimensional height of $H/D = 3.93$. Stainless steel combustor shell (AISI 316) has a wall thickness of 12.3 mm and is cooled by a matrix of impinging water sprays. Phase change of water at the outer wall removes heat from the combustor and keeps the wall temperature in the order of 100–200°C in order to prevent meltdown of the enclosure material. As a consequence, the combustion process in non-adiabatic, considering the heat flux through the wall and the radiative losses at the open exhaust. K1 grade kerosene fuel, which is quite close to standard Jet-A fuel in chemical composition, is injected through the center via a Parker-Hannifin Research-Simplex-Atomizer (RSA) nozzle with a cone angle of 26°. Lower heating value of kerosene fuel is 46300 kJ/kg. Its average chemical composition can be approximated as $C_{12}H_{24}$. The main combustion air is fed through a 45°-swirl vane with inner and outer diameters of 34 and 63 mm respectively (see Figure 2).

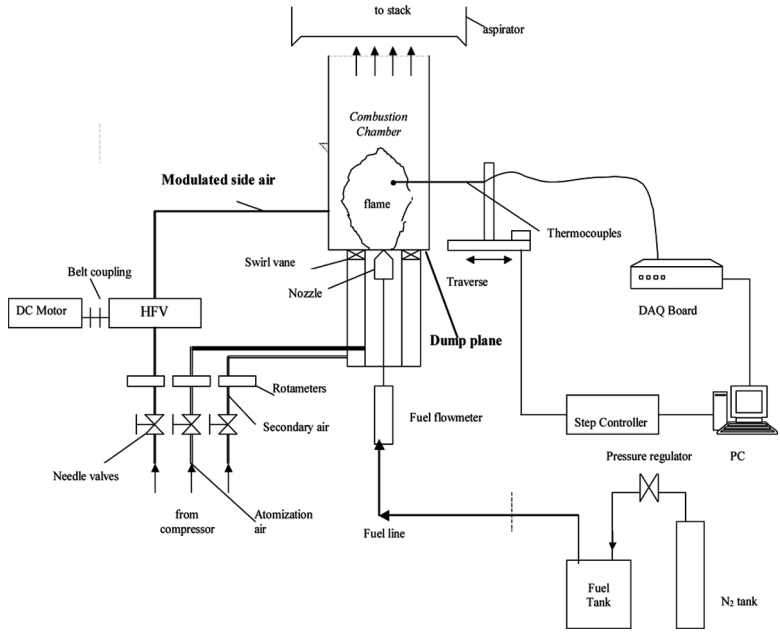

Figure 1. Schematic layout of the experimental apparatus.

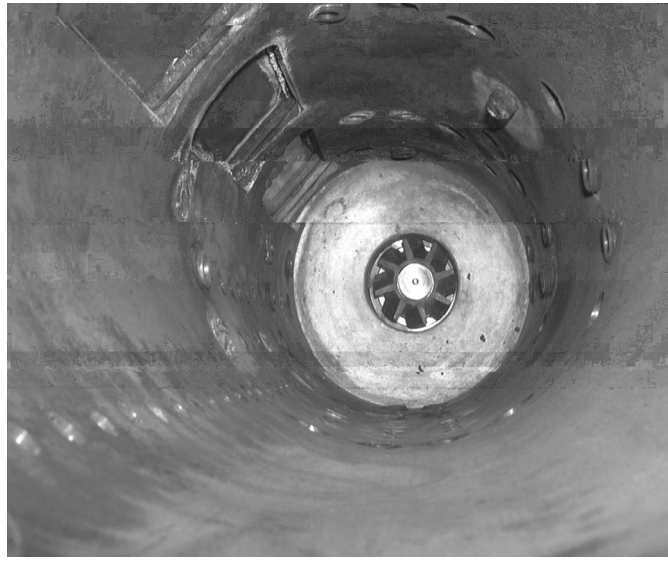

Figure 2. Inside view of the combustor.

An empirical correlation suggested by Beer and Chigier (1972) gives the corresponding swirl number as $Sw = 0.74$. The step height at the dump plane (i.e., sudden expansion at dump plane) is 65 mm. Flow over a back step establishes a re-circulation zone, which helps flame stabilization at the dump plane. A 38×64 mm quartz window on the shell enables optical access to the flame. A number of thermocouple ports are located at different elevations and angular locations, and type B Pt-Rh thermocouples are used to map the temperature distribution inside the combustor. Thermocouple wires are sheathed inside a twin-bore ceramic cladding of 3 mm outer diameter. Thermocouple signals were recorded using a 12-bit data acquisition board. A rake with two to four thermocouples mounted on an automated traverse is typically used for obtaining the temperature distributions inside the reactor. Temperature readings are averaged over a time period of 30 seconds and corrected for radiation losses using the method outlined by Bradley et al. (1961, 1968). An optically thin flame within the infrared spectrum is assumed for those calculations. A typical radiation correction for 600°C thermocouple recording is approximately 20°C and a correction of about 120°C is necessary for a thermocouple reading of 1000°C. Repeatability of the temperature measurements is found to be ± 20 K (Tuncer et al., 2003, 2005). In addition, fuel and airflow rates are obtained by a series of rotameters and pressure gauges. An overall uncertainty of $\pm 4.5\%$ in the equivalence ratio is estimated.

A Kistler 7061 water-cooled piezo-electric pressure transducer is mounted along the combustor wall and measures pressure variations in the combustor. Pressure spectrum in the frequency domain is computed with an SRS-785 spectrum analyzer.

Injection holes for side-air jets each having a diameter of 9.5 mm are uniformly distributed in the circumferential direction (see Figure 2). In this study, four injection holes ($n = 4$) located at an elevation z/D of 0.2 are used in order to modulate the main reaction zone. The circumferential location of the four injection holes is shown in Figure 3.

A spinning valve is used as the actuator in order to modulate the side-air jet flow. A spinner element with a number of holes drilled at the periphery is rotated inside a stationary enclosure, which has two stationary discharge holes. As the stationary holes on the enclosure and the spinning holes on the spinner element match successively the flow passing through the valve is modulated at a frequency dictated by the rotational speed of the spinner. Design uses a somewhat similar concept as in (Baroah et al., 2002), yet differs in geometry. Refer to Figure 4 for a basic sketch of the spinning valve arrangement. Further discussion on the design and performance of this particular actuator can be found in (O'Donnell, 2001). For the unmodulated baseline flow condition, the spinning valve is by-passed and the side-air jets are directly injected into

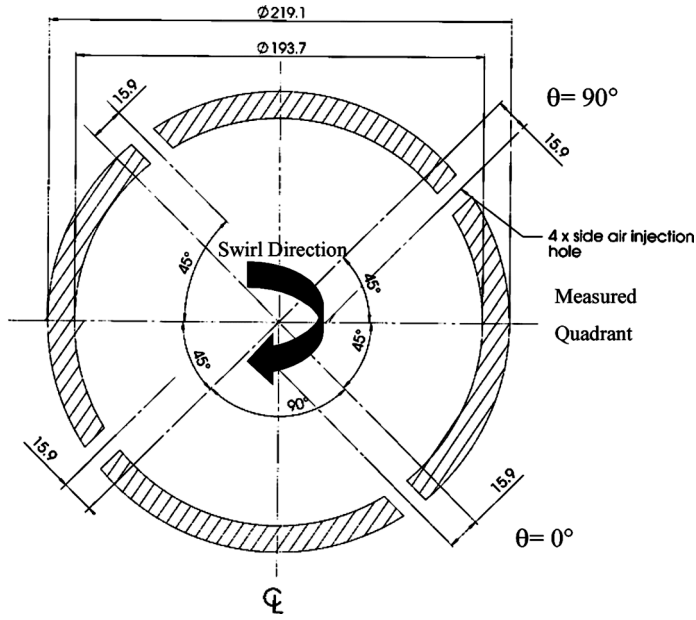

Figure 3. Section view of combustor at z/D = 0.2 (all dimensions in mm).

the combustor. Flow rate of air jets is independently monitored upstream of the spinning valve using a rotameter and a pressure transducer located in the feed tube. Flow rate at each forcing frequency is kept constant.

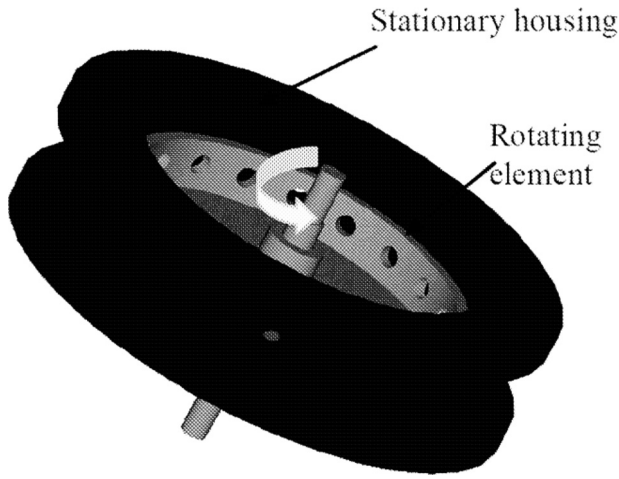

Figure 4. A basic sketch of spinning valve arrangement.

This is verified from the flow rate measurements upstream of the spinning valve. Furthermore, during calibration of the spinning valve with a hot-wire anemometer it is observed that mean flow velocity is not a function of the forcing frequency, which also suggests that the mean flow rate is indeed constant and does not change with the frequency.

Hot-wire anemometry measurements at the jet discharge clearly identify the periodicity of the velocity signal. Fourier spectrum of jet discharge velocity generates a strong peak at the modulation frequency. This reveals that flow is indeed modulated at the desired frequency. Harmonic peaks of lesser amplitude are also generated mainly due to non-linear acoustics of the flow conduits (Tuncer et al., 2005).

Figure 5 shows the forcing amplitudes of the frequencies used in this study on a logarithmic (dB) scale. Frequencies that possess similar high amplitude response within the frequency range of interest were chosen (100 Hz, 300 Hz and 600 Hz). Standard deviation of amplitude variation for the selected frequencies is 2.15 dB (about 2.5% of the forcing amplitude). Further experimentation with loudspeakers as actuators instead of the spinning valve (in order to adjust the amplitude freely by varying voltage) has shown that this amount of amplitude variation does not change the temperature reading more than the overall repeatability of thermocouple measurements (Tuncer et al., 2005). Therefore, the amplitude effects are factored out in the measurements.

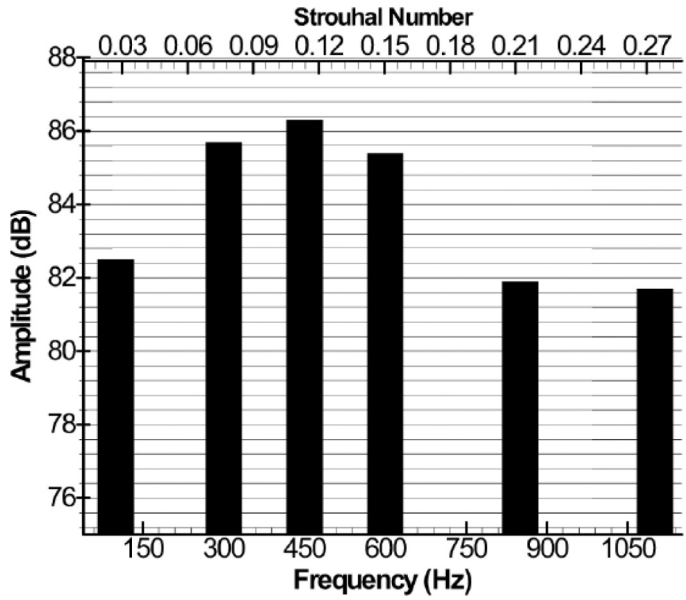

Figure 5. Relative forcing amplitude with respect to forcing frequency.

RESULTS

The combustor is operated over a number of load conditions to explore parametric variations within a large range of commonly reported values. These parameter (equivalence ratio, blowing ratio, forcing frequency) ranges include: ($0.62 < \phi < 1.00$, $4.4 < R < 10.8$, $0 < f < 850$ Hz). In all of the experiments both the combustion air and side-air jets are supplied to the combustor at an inlet temperature of 20°C and the operating pressure was 1 atm.

The majority of the detailed experiments (radial temperature and NO measurements) are made for a blowing ratio of 7.8 and equivalence ratio of 0.87. Preliminary studies on the other hand covered the whole parameter space described here. A table of flow conditions where more detailed measurements have been conducted (see Table 1) is presented below. Blowing ratio refers to the jet to cross flow velocity ratio. For these conditions, a constant kerosene flow rate of 2.4 g/s, primary combustion air and side air-jet flow rates of 29 l/s and 12 l/s are used. Hence the amount of side air jet flow is slightly under 1/3 of total air flow (side air + primary combustion air). These figures correspond to a thermal power rating of 111 kW assuming all fuel is consumed before the flow reaches the exit plane at z/D = 3.93. Adiabatic flame temperature corresponding load condition is roughly 1830°C, yet the combustor itself did not constitute to an adiabatic control volume during the experiments due to heat removal. At these flow rates, the jet Reynolds number $\mathrm{Re}_{jet} = u_{jet}L/\nu$, wher $L = (\dot{m}_{jet}u_{jet}/\rho U_\infty^2)^{1/2}$as suggested by Broadwell et al. (1984) is 1.4×10^6. Corresponding cross flow (main combustion air) Reynolds number $\mathrm{Re}_\infty = U_\infty D/\nu$ is 5.7×10^6 based on cold flow

Table 1. Flow conditions at which detailed measurements were conducted

Blowing ratio	Equivalence ratio	Jet forcing frequency
4.4	0.87	0
	0.87	300
6.3	0.87	0
	0.87	300
7.8	0.62, 0.68, 0.75, 0.87, 1.00	0
	0.62, 0.87, 1.00	100
	0.62, 0.68, 0.75, 0.87, 1.00	300
	0.62, 0.87, 1.00	450
	0.62, 0.87, 1.00	600
9.3	0.87	0
	0.87	300
10.8	0.87	0
	0.87	300

properties. For those measurements the equivalence ratio is kept constant by fixing the total airflow rate (i.e. an increase in jet mass flow rate is compensated by an equal amount of decrease in the cross-flow mass flow rate).

Pressure Spectra

The combustion chamber is acoustically closed at the inlet and open at the outlet. Consequently, the dominant acoustic mode of the combustion chamber corresponds to a quarter wave mode (Culick, 1976). This is clearly seen in the Fourier spectra of the pressure signal (see Figure 6) where there is a peak at the quarter wave mode ($f_{1/4} = c/4H$) around 225 Hz. Open loop forcing of the side air at 300 Hz is seen not to alter the dominant mode of combustion. The spectra clearly show both the quarter wave acoustic mode and the forcing frequency. The added mode due to open loop forcing at a constant frequency is responsible for the alteration of the temperature field and nitric oxide emissions.

Emissions Measurements

Nitric oxide emissions were measured using a chemiluminescence analyzer. A custom made water-cooled suction probe is inserted into the combustion chamber at an elevation near the exit plane (z/D = 3.9) where intrusion effect on the readings is negligible (Chen, 1995). Point wise measurements at the center have been made to cover the whole parameter space to provide

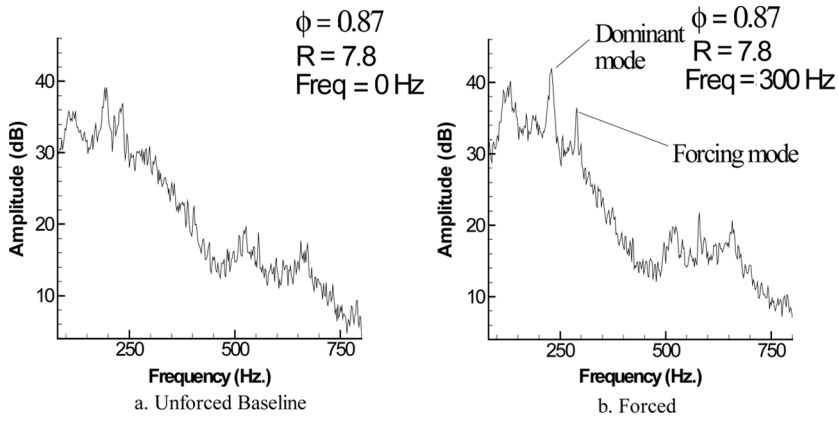

Figure 6. Pressure spectra at unforced and forced load conditions (pressure recorded at z/D = 0.4).

some a priori information for the detailed measurements. Radial NO concentration profiles at some of these load conditions have been selectively measured by traversing the suction probe in the radial direction. It is found that radial profiles and centerline measurements are consistent with each other. Absolute nitric oxide concentrations (ppm) are non-dimensionalized by converting them into an emission index EINO. Emission index of nitric oxide is defined as number of grams of NO generated per kg of fuel burnt. All of the EINO figures shown in the proceeding plots have been calculated using radially weighted averages assuming constant mass flux per unit area (density $\times$ velocity) at the measurement station which is located at the combustor exit. There are negligible temperature variations at the exit as it can be seen from the pattern factor plots. Turbulent velocity profiles are also fully developed at the NO measurement station. From these two arguments one can justify the assumption of constant mass flux per unit area.

There are several inter-related factors affecting the value of emissions index.

(1) Stoichiometry with higher emissions at near-stoichiometric conditions,
(2) Time-averaged temperatures with higher temperatures producing higher emissions,
(3) Reaction zone residence time with higher NO concentration associated with larger residence times,
(4) Unsteadiness-chemistry interactions with lower NO at higher unsteadiness levels.

Whether the side-air jets are pulsed or un-pulsed there will be additional swirl generated due to jet injection. With the addition of this secondary swirl the overall swirl number can increase. However beyond a critical value of $Sw = 0.5$, EINO is insensitive to changes in the swirl number (Chen, 1995). In this study since a higher swirl number is used ($Sw = 0.74$), possible effects on NO due to variations in swirl number with side-air jet modulation are unlikely. In this article authors have not performed any parametric study on the effect of swirl number on emissions as this issue has already been thoroughly investigated by other colleagues.

There are certain pathways to nitric oxide formation; thermal (via extended Zeldovich mechanism), prompt (via Feninmore mechanism (1979)) or due to fuel bound nitrogen. For the present case, there is no fuel bound nitrogen; therefore nitric oxide emission is generated by thermal and prompt mechanisms. Thermal NO is generated broadly in the high temperature regions all throughout the combustor, whereas prompt NO is mainly generated at the flame front (Westblom et al., 1994) where CH

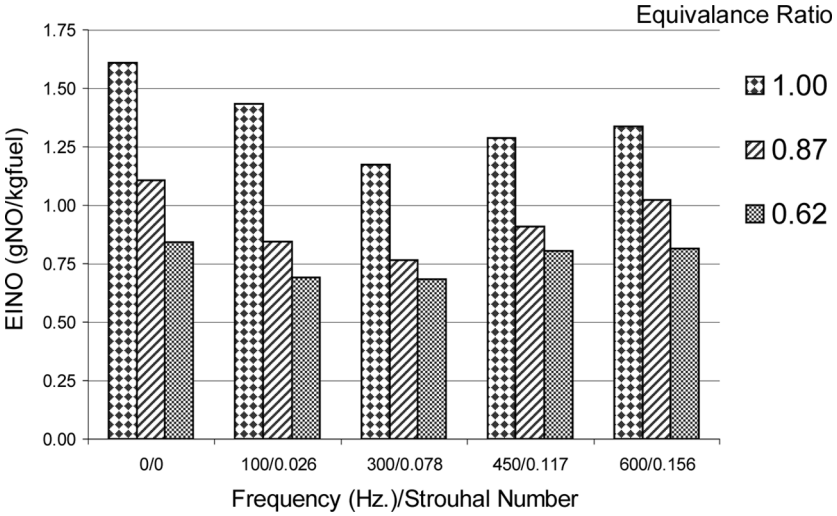

Figure 7. Effect of frequency on emissions index at R = 7.8.

and therefore HCN have higher concentrations. The emissions analyzer measures the total nitric oxide concentration without regard to the formation mechanism.

Figure 7 demonstrates the effect of forcing frequency on EINO at a constant blowing ratio of R = 7.8. Results are shown for the unforced case (0 Hz), and for forcing frequencies of 100 Hz, 300 Hz, 450 Hz and 600 Hz. Strouhal numbers are based on jet discharge hole diameter and jet velocity. Results are shown for three different global equivalence ratios ($\phi = 1.0$, 0.87 and 0.62). EINO values range from 0.70 to 1.60 gNO/kgfuel. Emission levels corresponding to unforced baseline cases are higher than corresponding forced condition at all three equivalence conditions. As side air jet forcing is introduced emissions decrease and attain a minimum value at 300 Hz at all three, load conditions. Typical reductions in EINO are around 30% at 300 Hz for equivalence ratios of $\phi = 0.87$ and 1. Beyond 300 Hz, EINO increases gradually back to the baseline level. Although not shown here, at 850 Hz for example, emission levels are almost the same with baseline levels.

Figure 8 demonstrates the effect of blowing ratio (the ratio between jet velocity to cross-flow velocity) on the emissions index. For all cases, the global equivalence ratio is kept constant at $\phi = 0.87$. Since the total airflow rate is the same for all cases, the mean residence time is likely to be similar for the various cases investigated. The addition of more flow through the side-air jets at z/D = 0.2 can slightly shift the combustion regime downstream therefore decreasing the mean residence time.

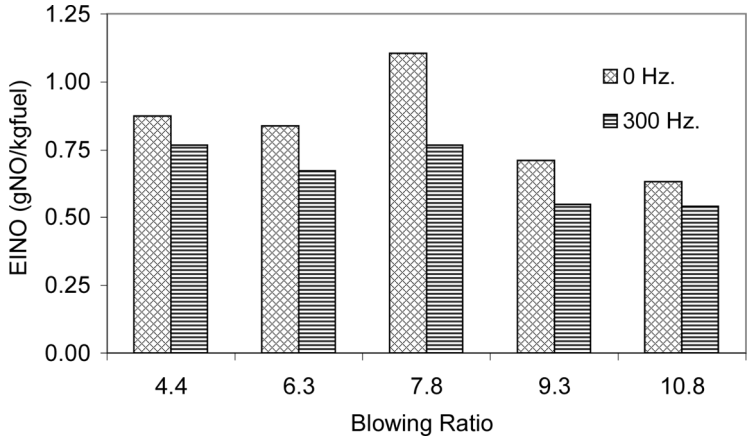

Figure 8. Effect of blowing ratio on emissions index at $\phi = 0.87$.

However, this reduction is quite minimal considering the distance between the jet injection location and the dump plane in comparison to combustor height. Nevertheless, higher blowing ratios will have a slight bias towards lower residence times (at most 10% reduction at $R = 15$). Only the baseline and 300 Hz forcing cases are shown in Figure 8 since the greatest reduction in EINO at all these blowing ratios is observed at 300 Hz. The EINO shows a significant peak at $R = 7.8$, and with jet modulation leads to a reduction in EINO of over 30%. At high blowing ratios ($R = 9.3$ and $R = 10.8$) EINO is lower than those obtained at low blowing ratios ($R = 4.4$ and $R = 6.3$). This can mostly be attributed to the quenching effect of high momentum side air jets and partially to a decreased residence time. When the momentum ratio J is high (e.g., 10.8), the associated high strain rates quench the reaction leading to local regions of lower temperature and thus lower NO production. Modulating the jet at 300 Hz leads to about a 15% reduction in EINO. On the lower end of the blowing ratio range, the jet to mainstream mass flow ratio and momentum ratio J is much lower. Therefore, authority of the jets over the whole flame is reduced. This accounts for the smaller percentage reduction (order of 13%) at $R = 4.4$ blowing ratio compared with the reductions achieved at the higher blowing ratios. These observations are consistent with isothermal cross flow mixing studies that show that forcing has a reasonably positive effect in terms of mixing for blowing ratios greater than 6 ($R \geq 6$) (Blossey et al., 2001; Narayanan et al., 2002). Therefore, blowing ratios larger than 6 have the needed "control authority" for control, and focusing attention for values of $R \geq 6$ is an appropriate choice for combustion control. By the phrase "control authority," the authors

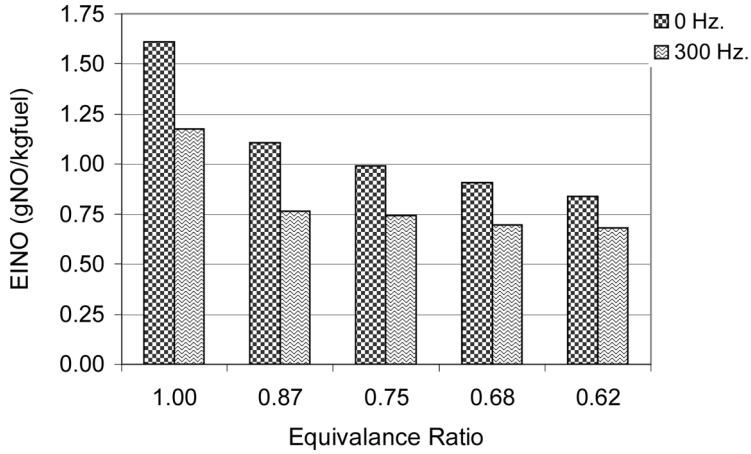

Figure 9. Effect of equivalence ratio on emissions index at R = 7.8.

refer to the ability of the modulated jet to influence the performance metrics of the combustor (e.g., emissions, volumetric heat release and pattern factor).

Figure 9 shows the effect of equivalence ratio on EINO at a blowing ratio of R = 7.8. This is the blowing ratio at which the maximum percentage reduction in EINO is obtained with forcing. Both baseline and 300 Hz forcing cases are shown. For each case emissions index rises towards stoichiometric flow condition as expected. Emissions are typically highest at near stoichiometric conditions. Although rich flow conditions are not explored here emission levels are expected to drop, as flame gets richer and richer (due to incomplete combustion and thus lower temperatures).

Figure 10 shows the percentage reduction in emissions index at 300 Hz forcing with respect to unforced baseline. A maximum reduction of about 30% with respect to unforced baseline condition is obtained at a blowing ratio of R = 7.8. A 13–30% reduction in emissions index over the whole blowing ratio range can be obtained. Interestingly, at each blowing ratio, the 300 Hz forcing yielded the maximum reduction for most of the load conditions that were studied during the experiments. These findings suggest that in defining the Strouhal number, the jet diameter and the jet velocity are not the appropriate scaling parameters. For example while keeping the global equivalence ratio constant at different blowing ratios the jet discharge velocity is varied. Even though the jet discharge velocity was changed and jet diameter is constant the 300 Hz forcing consistently showed the best improvement. Over this range of blowing ratios optimal Strouhal number (in terms of NO emissions) varies considerably. This supports the previous argument that the jet

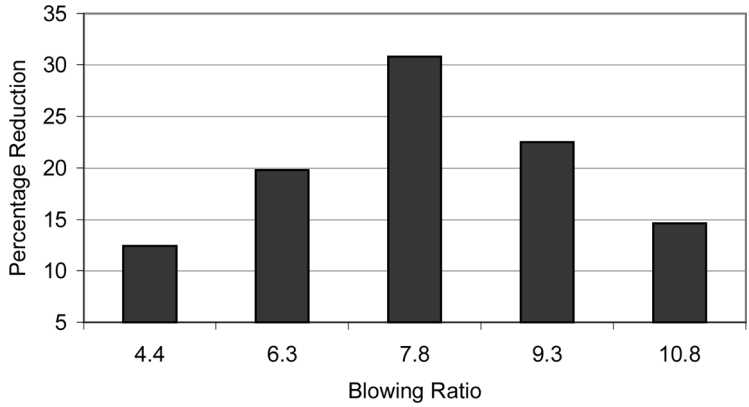

Figure 10. Percentage reductions in emissions index with respect to unforced baseline (corresponding to Figure 7).

diameter and the jet velocity are not the appropriate scaling parameters for non-dimensionalization of the results.

Figure 11 shows the radial NO concentration for different forcing frequencies at $R = 7.8$ and $\phi = 0.87$. The baseline and four other forcing frequencies are shown. NO concentration is higher near the center and decreases towards the combustor wall. It is seen that nitric oxide concentration at 300 Hz forcing frequency is lower than the baseline case at almost all radial locations. Reductions of smaller magnitude are obtained at other frequencies (e.g., 100 Hz.). At forcing frequencies higher than 300 Hz, the emission levels begin approaching the baseline case, and at off-center radial locations the emission levels can even exceed the baseline levels. Therefore, high frequency forcing is generally of no interest in terms of nitric oxide emissions.

Figure 12 shows radial profile of NO concentration at a blowing ratio of $R = 6.3$. Only baseline and 300 Hz forcing conditions are plotted. NO concentration again reduces towards the combustor wall. With forcing NO concentration is significantly reduced at all measurement stations with reduction levels ranging from 15–25% (and an average reduction of 20% as shown in Figure 11). Both Figures 10 and 11 indicate a consistent pattern between the centerline values and the radially averaged values.

Temperature Profiles

In this section three dimensional time averaged temperature results are presented at a selected load condition. Measuring the temperature

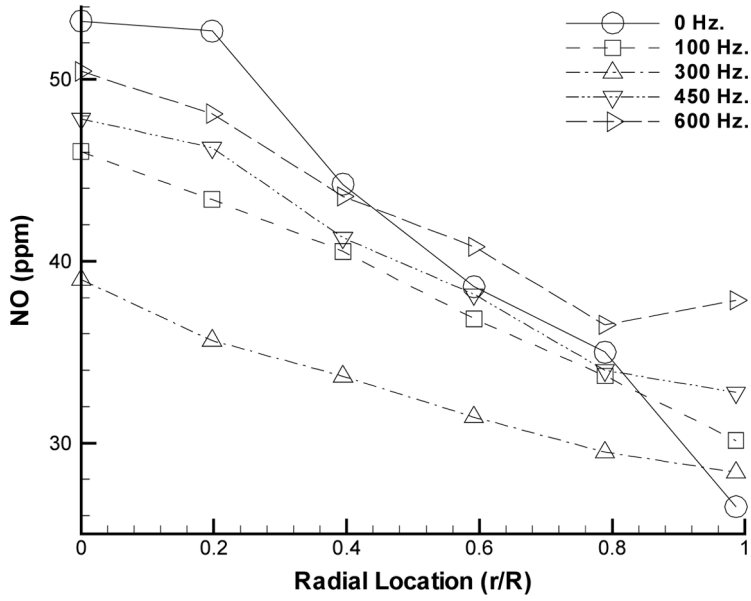

Figure 11. Radial profile of absolute NO concentration at R = 7.8 with frequency as a parameter ($\phi = 0.87$).

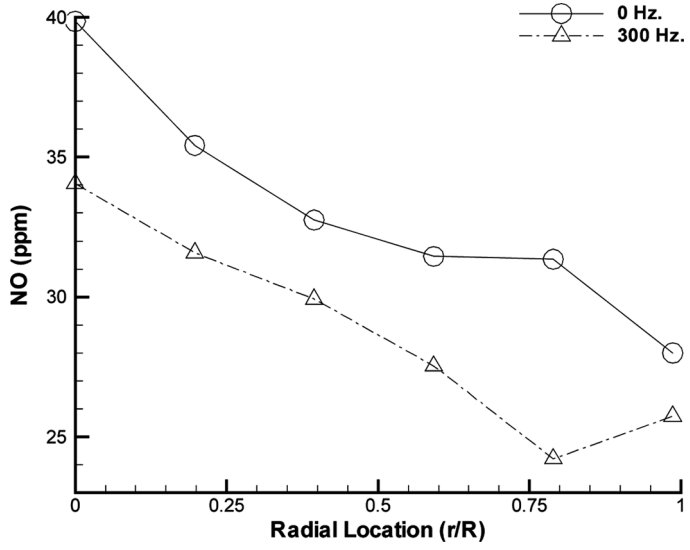

Figure 12. Radial profile of absolute NO concentration at R = 6.3 and ($\phi = 0.87$).

distribution is one way to quantify fuel air mixing. The degree of mixing can itself be inferred from the uniformity of temperature profiles. Greater mixing will lead to a more uniform temperature profile. While NO formation depends on temperature, the time averaged temperature field is not the only measure controlling the emission levels. There are several other factors such as the unsteadiness and mean residence times that can play a role in the NO formation process.

Prior to a formal discussion it is useful to state the quantities relevant to the flow conditions used to generate data shown in Figures 13 to 15. The front-end equivalence ratio (based on air delivered only through the front-end) is $\phi = 1.2$. Global equivalence ratio (based on total air) is held constant at $\phi = 0.87$ with a procedure described earlier in the text. Only the baseline and 300 Hz modulation results are shown. Recall that 300 Hz forcing yielded the minimum amount of nitric oxide emission for this particular flow condition (see Figure 11). Dimensionless frequency corresponding to 300 Hz jet forcing is $St = 0.069$.

Figure 13 shows temperature contours at different elevations. These temperature contours are shown only for one quadrant of the combustor, between the two side air-jets. Note that side air-jets are introduced at $z/D = 0.2$, and the axial locations shown in Figure 13 ($0.3 \leq z/D \leq 1.1$) are downstream of the side air-jet injection location (the lowest plane presented is at $z/D = 0.3$) where the influence of the side air-jets on the fuel-air mixing is the most significant. One should note that combustion

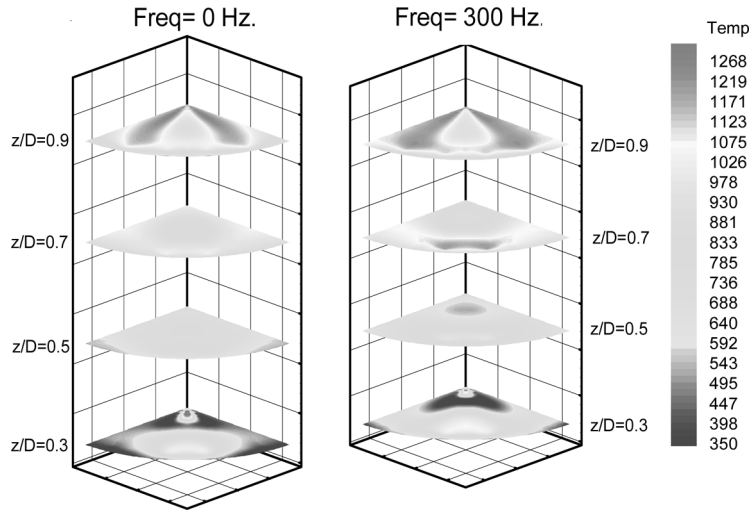

Figure 13. 3-D temperature contours at $R = 7.8$ and $\phi = 0.87$ (Temperatures in $^{\circ}C$).

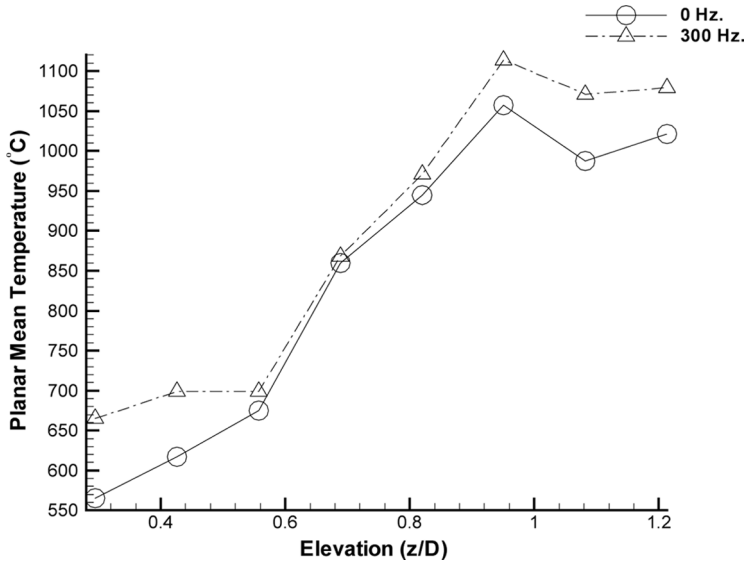

Figure 14. Planar mean temperature as a function of elevation at R = 7.8 and $\phi = 0.87$.

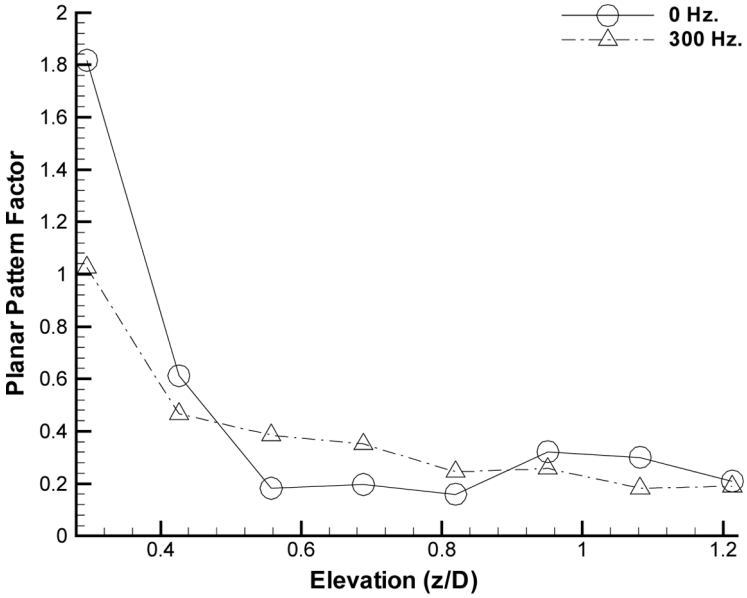

Figure 15. Planar pattern factor as a function of elevation at R = 7.8 and $\phi = 0.87$.

continues to occur further downstream, and at the exit (z/D = 3.93), the mean stack temperatures for the modulated and unmodulated cases are the same.

Immediately following injection at z/D = 0.3, for the unmodulated case, it is seen that jet fluid is located at the flame periphery near the combustor wall marked by a blue cold region. Consequently, jet penetration, and mixing is poor. With modulation, the temperatures in the cold region near the combustor wall are increased as jet mixes better with the reacting cross flow. At this elevation, z/D = 0.3, and at higher elevations, planar mean temperatures are higher in the modulated case. This is a consequence of the enhanced fuel-air mixing induced by the modulation. Local enhancements in temperatures as large as 250°C can be observed; however, at each z/D, the average enhancements appear to be more in the range of 50–75°C.

Figure 14 shows mean temperature $\overline{T}$ as a function of non-dimensional height (z/D). Data used to generate this plot was shown earlier in Figure 13. Immediately downstream of the jet injection ($0.2 < z/D < 0.6$), planar mean temperatures rise quickly for the modulated case (300 Hz forcing frequency). This is associated with increased volumetric heat release and kerosene burns more rapidly within the same downstream distance.

Pattern Factors

Uniformity of the temperature profiles and thus air fuel mixedness can be quantified by defining a pattern factor. A planar pattern factor (PF) is defined in the present article as follows:

$$PF(z) = \frac{T_{\max}(z) - \overline{T}(z)}{\overline{T}(z) - T_o} \tag{1}$$

where the radially-weighted average temperature $\overline{T}(z)$ is representative of the mean temperature in the (r,θ) plane. This is computed from the finite sum representation of the following equation;

$$\overline{T}(z) = \frac{\int\int T(r,\theta,z) r dr d\theta}{\int\int r dr d\theta} \tag{2}$$

Lower pattern factor values indicate a more uniform distribution, with less variance in the temperature profile (Tuncer et al., 2003, 2005), and is desirable from the perspectives of lower emissions.

Figure 15 shows the planar pattern factors plotted versus non-dimensional height (z/D) measured from the dump plane for the baseline and the 300 Hz forcing cases. The pattern factor PF decreases with

downstream distance due to increased mixing. Downstream of the jet injection, a substantial reduction in the pattern factor (e.g. from 1.8 to 1.0) is observed with modulation. Counter-intuitively, this is accompanied by a simultaneous increase in temperature (Figure 13). This observation indicates that both the uniformity of the temperature field and the temperature levels can be favorably altered with flow modulation. Moreover, forcing effects are observed to be relatively stronger in the primary combustion region ($z/D < 0.6$) and close to jet injection location ($z/D = 0.2$). However, between $0.6 < z/D < 0.8$ baseline pattern factors are observed to be lower than the ones at 300 Hz modulation case. Further downstream, at $z/D = 1.2$, both pattern factors are nearly the same at $PF = 0.2$.

DISCUSSION

Temperature distributions shown in Figure 12 are counter-intuitive with the NO emission data in Figures 6 and 8. These plots indicate that forcing at 300 Hz leads to higher average temperatures at each axial plane (Figure 12), and at the same time produces a reduction in NO levels (Figure 8). It is well accepted that NO and mean temperatures have a direct correlation with each other. However, NO emissions are also known to depend on other factors (as mentioned earlier) such as residence times and unsteadiness, and clearly in the present study, these factors play an important role. The NO emission results presented thus far cannot therefore be attributed to just the mean temperature. As far as the temperature effects are concerned reduced local equivalence ratio/hot spots can lead to decreased emissions index values.

As mentioned earlier, pollutant formation chemistry is closely coupled with turbulence (or temporal fluctuations). Since the jet injection is of oscillatory nature and jet is injected right into the main reaction zone, where most of nitric oxide is formed, it causes the flame boundary (and flame volume V_{flame}) to fluctuate. Modulated jet injection adds another cyclic mode to flame (Tuncer et al., 2003, 2005), leading the flame to stretch and contract along the axis of the side air jet. This means that the residence time, which is related to flame volume ($\tau_R \alpha V_{flame}$), also has a fluctuating component at the jet frequency. Chen et al. (1995) have found that EINO scales with the square root of the Damkohler number (i.e., $EINO \ \alpha \ Da^{0.5}$) over four decades of Reynolds numbers. Since $Da = \tau_R/\tau_{NO}$, unsteadiness in τ_R leads to fluctuations in Da ($Da(t) = \overline{Da} + Da'(t)$). Due to the nonlinear EINO $\sim$ Da relationship, the time averaged EINO will depend not only on the time averaged $\overline{Da}$, but also on the fluctuating component $Da'(t)$ since $EINO \ \alpha \lim_{T\to\infty} \frac{1}{T}\int_0^T \left(\overline{Da} + Da'(t)\right)^{0.5} dt \neq \overline{Da}^{0.5}$. For this reason, the time-averaged

EINO levels in Figure 8 cannot be directly correlated with the time averaged temperature distributions in Figure 15.

Furthermore recently Santoro et al. (2002) studied nitric oxide formation during flame vortex interaction with a methane diffusion flame. They concluded that vortex interaction did not significantly affect carbon monoxide mass fraction. On the other hand they show that vortex interaction and its characteristic time scale has a large impact on nitric oxide mass fraction. Their findings also indicate that the characteristic time of the vortex affects different NO formation paths differently. Thermal NO mass fraction was heavily dependent on the vortex timescale whereas no effect was observed for prompt NO. Prompt NO has a typical formation timescale of one millisecond. Timescales of forcing used in this study (ranging from 1.6 to 10 milliseconds) match that of extended Zeldovich mechanism. The 300 Hz forcing case where most significant reductions are obtained corresponds to a timescale (of the order of 3 milliseconds).

CONCLUSION

An experimental study is conducted to identify the potential of side air-jet modulation in a non-premixed swirl-stabilized spray-combustor to enhance volumetric heat release (leading to more compact combustors) and to lower emissions. Varying the forcing frequencies optimizes the mixing behavior of the modulated jets and emissions levels, and it is found that forcing at 300 Hz ($St = 0.069$ at a blowing ratio of $R = 7.8$) produces the lowest emissions. At the modulation frequency of 300 Hz, the volumetric heat release is also enhanced leading to higher temperatures. At the same time substantial reductions in the emission index (usually 15–30% depending on the flow condition) with respect to the unforced baseline condition can be achieved as well. The highest EINO values are achieved for a blowing ratio of 7.8, and the greatest reduction in EINO with modulation (>30%) is also achieved at this blowing ratio.

In the present study it is observed that the emissions levels are significantly reduced despite higher volumetric heat release and higher mean temperatures. Thus both performance metrics (volumetric heat release and emissions) are improved. This counterintuitive result is a consequence of the dependence of EINO on the modulation-induced unsteadiness in the flame volume and residence time in the primary high-temperature flame region.

To achieve suitable control authority, the forcing must directly impact the main reaction zone, and must impose pressure and heat release fluctuations that are at least as strong as those coming from the dominant acoustic modes of combustion. This requires modulation close to the dump plane ($z/D = 0.2$ in the present case) and an optimal

blowing ratio. In the present study it was observed that the blowing ratio should be in the range of R = 6–9 for achieving the most beneficial impact on emissions. Forcing frequencies in the range of 100–300 Hz (St = 0.026–0.069) were found to produce the most substantial effects. The emissions do not respond to high frequency oscillations due to potential mismatch with the nitric oxide formation time-scale.

NOMENCLATURE

D	Combustor diameter
H	Combustor height
z	Elevation measured from the dump plane
r	Radial coordinate
Sw	Swirl number
f	Frequency
U	Axial velocity
n	Number of jet injection holes
St	Dimensionless frequency $St = fd/u_{jet}$
F/A	Fuel to air ratio
R	Blowing ratio $R = u_{jet}/U_{\infty}$
n	Number of jet injection holes
S	Stoichiometric condition
PF	Pattern factor
T	Temperature
d	Orifice diameter
c	Speed of sound $c = \sqrt{\gamma RT}$
J	Momentum flux ratio $J = R^2 \frac{\rho_{jet}}{\rho_{\infty}}$
L	Length scale
M	Mach number $M = \frac{U}{c}$
Da	Damköhler number $Da = \tau_R/\tau_{NO}$
$\dot{m}$	Mass flow rate
[.]	Concentration
.	Placeholder
EINO	Nitric oxide emissions index gNO/kgfuel
t	Time

Greek Symbols

γ	Specific heat ratio
θ	Azimuthal position
ϕ	Equivalence ratio $\phi = \frac{(F/A)_{actual}}{(F/A)_{stochiometric}}$
τ	Time scale
ν	Kinematic viscosity
ρ	Density

Subscripts

c	Characteristic
max	Maximum
o	Inlet
jet	Side air jet
∞	Main flow
1/4	Quarter wave mode
NO	Nitric oxide
R	Global residence
flame	Flame
eq	Equilibrium

Superscripts

$^-$	Average

REFERENCES

Baroah, P., Anderson, T.J., and Cohen, J.M. (2002) Active Combustion Instability Control with Spinning Valve Actuator. ASME Paper No: GT-2002-30042.

Beer, J.M. and Chigier, N.A. (1972) Combustion Aerodynamics, Applied Science Publishers, London, United Kingdom, p.100.

Bicen, A.F., Tse, D.G.N., and Whitelaw, J.H. (1990) Influence of Air/Fuel Ratio and Swirl Number on the Combustion Characteristics of a Model Combustor. International Gas Turbine and Aeroengine Congress and Exposition, Brussels, ASME Paper No. 90-GT-411, pp. 1–11.

Blossey, P.N., Narayanan, S., and Bewley, T.R. (2001) Dynamics and Control of Jets in Crossflow Direct Numerical Simulations and Experiments. Proceedings of IUTAM Symposium on Turbulent Mixing and Combustion.

Bradley, D. and Entwistle, A.G. (1961) Determination of emissivity, for total radiation, of small diameter platinum-10% rhodium wires in the temperature range 600–1450°C. *Br. J. Appl. Phys.*, **12**, 708–711.

Bradley, D. and Matthews, K.J. (1968) Measurement of high temperatures with fine wire thermocouples. *J. Mech. Eng. Sci.*, **10**, 299–305.

Broadwell, J.E. and Breidenthal, R.E. (1984) Structure and mixing of a traverse jet in incompressible flow. *J. Fluid Mech.*, **148**, 405–412.

Chen, J.Y., Chang, W.C., and Koszykowski, M. (1995) Numerical simulation and scaling of NO_x emission from turbulent hydrogen jet flames with various amounts of helium dilution. *Combust. Sci. Technol.*, **110**, 505–529.

Chen, R.H. (1995) Some characteristics of NO_x emission of turbulent nonpremixed hydrogen air flames stabilized by swirl generated flow recirculation. *Combus. Sci. Technol.*, **110**, 443–460.

Cho, S.K., Yoo, J.Y., and Choi, H. (1998) Vortex pairing in an axisymmetric jet using two-frequency acoustic forcing at low to moderate Strouhal numbers. *Exper. Fluids*, **25**, 305–315.

Cortolezzi, L. and Karagozian, A.R. (2001) On the formation of counter-rotating vortex pair in traverse jets. *J. Fluid. Mech.*, **446**, 347–446.

Crocker, D.S., Smith, C.E., and Myers, G.D. (1994) Pattern Factor Reduction in a Reverse Flow Gas Turbine Combustor Using Angled Dilution Jets. Proceedings of the International Gas Turbine and Aeroengine Congress and Exposition, Hague, ASME Paper No. 94-GT-406, pp. 1–10.

Culick, F.E.C. (1976) Non-linear behavior of acoustic waves in combustion chambers. *Acta Astro.*, **3**, 715–734.

Feninmore, C.P. (1979) Studies of Fuel-Nitrogen Rich Flame Gases. 17th International Symposium on Combustion, The Combustion Institute, p.661.

Griebel, P., Fischer, M., Hassa, C., Magens, E., Nannen, H., Winandy, A., Chrysostomou, A., Meier, U., and Stricker, W. (1997) Experimental Investigation of an Atmospheric Rectangular Rich Quench Lean Combustor Sector for Aeroengines. Proceedings of the 1997 International Gas Turbine and Aeroengine Congress and Exposition, Orlando, ASME Paper No. 97-GT-146, pp. 1–8.

Holdeman, J.D. (1993) Mixing of multiple jets with a confined subsonic crossflow. *Prog. Energy Combust. Sci.*, **19**, 31–70.

Holdeman, J.D., Liscinsky, D.S., Samuelson, G.S., Oechsle, V.L., and Smith, C.E. (1996) Mixing of Multiple Jets with a Confined Subsonic Crossflow in a Cylindrical Duct, ASME Paper No. 96-GT-482.

Johari, H., Pacheco-Tougas, M., and Hermanson, J.C. (1999) Penetration and mixing of fully modulated turbulent jets in crossflow. *AIAA J.*, **37**(7), 842–850.

Kim, H.S., Baek, S.W., and Yu, M.J. (2001) Formation of nitric oxide in a multi-air staged gas flame. *Combust. Sci. Technol.*, **166**, 41–66.

Lilley, D.G. (2002) Jet Injection into Swirling Cross Flow for Improved Mixing and Combustion. Proceedings of the 2002 International Joint Power Generation Conference. pp. 881–888.

McLoskey, R.T., King, J.M., Cortelelezzi, L., and Karagozian, A.R. (2002) The actively controlled jet in cross flow. *J. Fluid Mech.*, **452**, 325–335.

McManus, K. and Lo, E. (1995) Closed-loop System for Control of Combustor Pattern Factor. Proceedings of the 1995 IEEE Conference on Control Applications, Albany, pp. 699–704.

Narayanan, S., Barooah, P., and Cohen, J.M. (2002) Experimental Study of the Coherent Structure Dynamics and Control of an Isolated Jet in Cross Flow. 40th Aerospace Sciences Meeting and Exhibit, Reno, Nevada.

O'Donnell, M. (2001) Spray Combustion Laser Diagnostics and Combustion control Via Air Flow Fluctuations, Louisiana State University, Baton Rouge, LA.

Santoro, V.S., Kyritsis, D.C., Smooke, M.D., and Gomez, A. (2002) Nitric Oxide Formation during Flame Vortex Interaction. *Proc. Combust. Instit.*, **29**, 2227–2233.

Tuncer, O., Acharya, S., Banaszuk, A., and Cohen, J. (2003) Side Air Jet Modulation for Control of Heat Release and Pattern Factor, ASME Paper No: GT2003-38853, pp. 603–611.

Tuncer, O., Acharya, S., Banaszuk, A., and Cohen, J. (2005) Side air jet modulation for control of heat release and pattern factor. *Combust. Sci. Technol.*, **177**, 1339–1364.

Vermeulen, P.J., Odgers, J., and Ramesh, V. (1982) Acoustic Control of Dilution-Air Mixing in a Gas Turbine Combustor. ASME Paper No. 82-GT-35.

Vermeulen, P.J., Ramesh, V., and Yu, W.K. (1986) Measurements of entrainment by acoustically pulsed axisymmetric air jets. *J. Eng. Gas Turb. Power*, **108**, 479–484.

Vermeulen, P.J. and Yu, W.K. (1985) An Experimental Study of Mixing by an Acoustically Pulsed Axisymmetrical Air Jet. ASME Paper No. 85-GT-49.

Westblom, U., Alonso, F.F., Mahon, C.R., Smith, G.P., Jeffries, J.B., and Crosley, D.R. (1994) Laser-induced fluorescence diagnostics of a propane/air flame with a manganese fuel additive. *Combust. Flame*, **99**, 261–268.